JOURNAL OF MATERIALS SCIENCE **35** (2000) 1715–1723

# Low cycle fatigue behaviour of particulate reinforced metal matrix composites

M. J. HADIANFARD*,‡, YIU-WING MAI§
*Centre for Advanced Materials Technology (CAMT) and §Department of Mechanical and Mechatronic Engineering (J07), University of Sydney, NSW 2006, Australia
E-mail: hadianfa@succ.shirazu.ac.ir

The low cycle fatigue (LCF) resistance of two different 6061 Al/20 vol% alumina particulate metal matrix composites (MMCs) in a peaked-aged condition has been evaluated under fully reversed strain control testing. Test results were combined with scanning electron and optical microscopy investigations to determine the effects of reinforcement particles and strain amplitude on the LCF behaviour of these MMCs. Both materials show three stages of response to LCF: initial fast hardening or softening in the first few cycles; gradual softening for most of the fatigue life; and a rapid drop in the stress carrying capability prior to failure. Both MMCs exhibit short LCF life which follows a Coffin-Manson relationship. All tested specimens demonstrate ductile fracture morphology at final failure. The experimental results are discussed in respect of strain amplitude, matrix composition and reinforcement shape and crack initiation. 

## 1. Introduction

Metal matrix composites (MMCs) are promising materials for lightweight, high strength structural applications. In particulate MMCs non-metallic particles are incorporated in metallic alloys to improve their elastic modulus and strength. However, introducing reinforcement particles with high modulus to the matrix alloy can reduce the fracture toughness [1] and change the fatigue resistance of the material. The effects of reinforcement on cyclic fatigue damage and crack initiation, its role on constraining matrix plastic flow during cyclic deformation and the response of the material are important aspects in low cycle fatigue (LCF) of MMCs.

The effect of non-metallic particles as inclusions on fatigue crack initiation of metallic alloys is well established [2]. For example calcium aluminates and alumina particles in steel played an important role to reduce the fatigue life [3, 4]. Knott *et al.* [5] found that non-metallic particles could influence the fatigue behaviour of conventional alloys in a number of ways: crack initiation, short crack growth and growth of a long crack. Toda [6] observed faster short fatigue crack intiation in a metal matrix composite, compare to its unreinforced matrix. Hurd [7] studied low cycle fatigue of Al-Mg-Si and Al-Si composites and unreinforced alloys. He found that the Al-Si composite was weaker than the unreinforced material due to the addition Saffil fibres and its LCF properties were also inferior. In the case of fibre reinforced Al-Mg-Si alloys the LCF properties were however comparable to plain alloys. Hassen *et al.* [8] studiedLCF and high cycle fatigue (HCF) of several particulate and whisker reinforced 6061 Al alloys. While the composites showed superior properties in HCF, no particular advantage was observed over the unreinforced alloy in low cycle fatigue. Harris [9] showed that in the case of Saffil fibre reinforced Al-Cu-Mg alloy, where the yield strength of the composites exceeded that of the unreinforced alloy, their fatigue strengths for both HCF and LCF were superior. Otani *et al.* [10] studied cyclic fatigue degradation and cumulative fatigue damage in an aluminum alloy reinforced with 20 vol% SiC by using LCF tests. It was found that fatigue damage is cumulative in the tested MMC and fatigue process of the material is governed by the internal crack density. A study of fatigue crack initiation in a titanium matrix composite [11] concluded that the fatigue crack growth resistance of the composite in the short-crack region was controlled by the fibre fracture and matrix work hardening near the fractured fibre. Perng *et al.* [12] reported poor LCF behaviours of different volume fraction alumina reinforced 6061 Al matrix when compared to their unreinforced matrix at room and elevated temperatures. Levine *et al.* [13] tested low cycle fatigue properties of unreinforced 6061 Al, 15 vol% SiC particulate reinforced 6061 Al and 20 vol% of short Saffil fibre in 6061 Al. They found that at low strain amplitudes the particulate composites showed the largest tolerance against plastic strain cycling. But at high strain amplitudes the unreinforced matrix was superior to the composites. Bhatt and Grimes [14] investigated the low cycle fatigue behaviour of 25 and 44 vol% $SiC_f$/Ti MMCs and found that their fatigue life was reduced compared to the unreinforced material at a given stress amplitude. Robles *et al.* [15] reported that, at low

‡ *Present address*: Department of Materials Science and Engineering, School of Engineering, Shiraz University, Shiraz, Iran.

strain amplitudes, the fatigue lifetimes of a copper alloy strengthened by dispersed oxide particles and the plain alloy were similar. However the former was more susceptible to cracking at stress concentration sites. Llorca *et al.* [16] studied the LCF behaviour of an Al-3.5%Cu alloy reinforced with 0, 6, 13 and 20 vol% SiC particulates. It was shown that although the monotonic deformation of the composite was strongly influenced by the volume fraction of SiC reinforcement, the cyclic deformation was relatively unaffected. Elzey and Arzt [17] demonstrated that the presence of non-metallic dispersoids in nickel-based alloy suppressed crystallograpic micro-cracking thereby improving the low cycle fatigue life of the composite compared to the plain alloy.

For efficient use of MMCs a comprehensive understanding of their behaviour under cyclic stresses must be obtained. Therefore, the aim of this work was to determine the resistance of particulate MMCs subjected to repeated straining and to evaluate those factors that might affect their low cycle fatigue (LCF) behaviour.

## 2. Experimental work

### 2.1. Materials

Two different particulate metal matrix composites were used in this work. The first composite material was Duralcan-20% (D20), a 6061 aluminum alloy reinforced with 20 vol% angular alumina particles. The second composite was Comral-85 (C85), a 6061 aluminum alloy reinforced with 20 vol% alumina microspheres. Fig. 1a and 1b show the microstructures of these materials. Both materials were tested in peak-aged (T6) condition. To produce peak-aged material the specimens were subjected to the following heat treatments: solution heat treated at 530 C for 1.5 h, then cold water quenched, and natural aged at room temperature for 24 h which was followed by artificial ageing at 175 C for 8 h.

### 2.2. Fatigue specimens

Since the materials were extruded plates of 75 mm width and 25 mm thickness, a rectangular cross-section specimen with a gauge length 12.5 mm was selected. The fatigue specimens were fabricated with the gauge length parallel to the extrusion direction, and with dimensions according to ASTM E606-92. During machining, care was taken in obtaining a surface finish with minimum damage or distortion. The machined surfaces of the specimens were ground with 1200 grit silicon carbide paper and then mechanically polished to 1 $\mu$m by diamond-based polishing compound. The specimens were polished parallel to the load axis until a smooth scratch-free surface was obtained. After polishing the thickness and width of the specimens were measured by an optical projector with $\times 20$ magnification. A layer of cellophane tape was applied around the specimen at the knife edge contact points to reduce slippage of the knife edges and prevent surface damage of the specimen by the extensometer.

### 2.3. Low cycle fatigue fixture

One of the most critical aspects of strain-controlled fatigue testing is the alignment of the specimen. Any misalignment in applied load produces a bending moment and causes experimental error. Therefore the fixture has an important role in alignment and load transfer. The alignment was also monitored by strain gauges mounted on both sides of the specimen. When satisfactory alignment was achieved, the fixture was then fastened. The test specimen was friction-gripped by steel plates tightened with four bolts on each half and was positioned to enable the specimen axis to pass through the centre of fixture (see Fig. 2). A maximum bending strain of no more than 4% of the minimum axial strain was permitted at all times during testing.

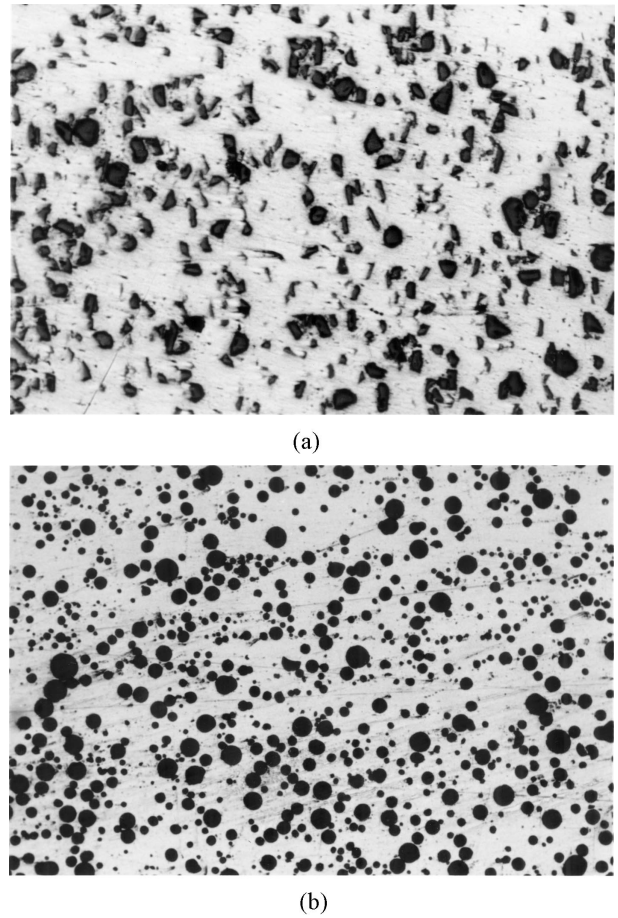

*Figure 1* Microstructure of (a) D20 (200×) (b) C85 (200×).

### 2.4. Test procedures

All low cycle fatigue tests were performed at room temperature under laboratory conditions and fully reversed strain-controlled tension-compression with a stress ratio $R = -1$. The specimens were subjected to strain-controlled uniaxial cyclic loading in an Instron 8501 machine, which utilised a closed loop servo-hydraulic system, with 100 KN load cell capacity.

An Instron dynamic electromechanical strain extensometer model 2620-602 with strain range $\pm 20\%$ was used for measuring the longitudinal deformation. The mean strain was zero and strain function exhibited a sinusoidal wave form. A cyclic frequency of 0.4 c/s was employed for all tests.

The cyclic response of the material was monitored in real time through a computer-controlled data acquisition system. Both the load and displacements were simultaneously and continuously recorded. To determine the LCF behaviour of materials, 10 specimens were

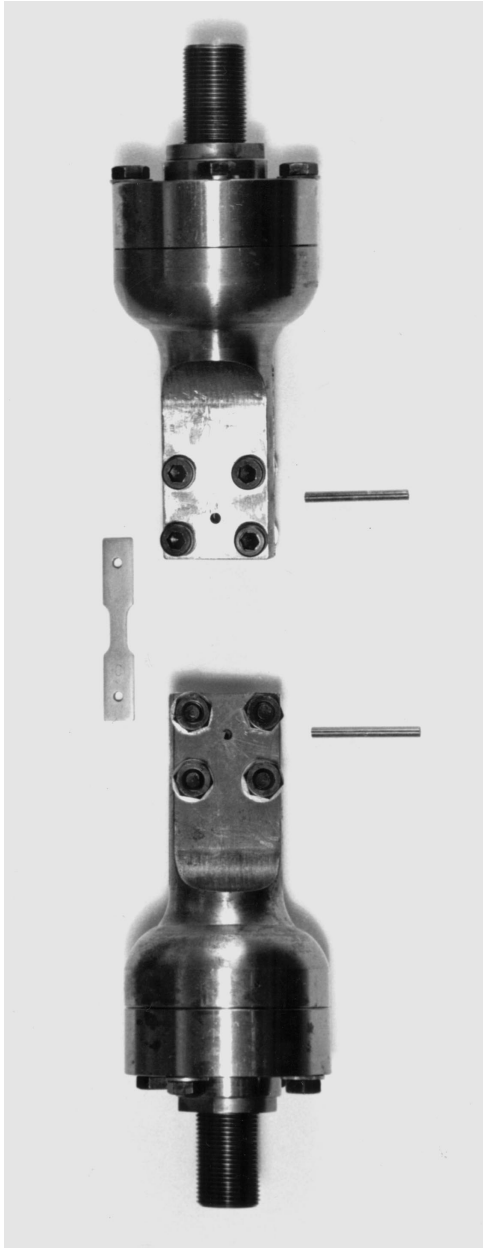

*Figure 2* Experimental fixtute for LCF test.

tested from each composite material. The strain amplitude at which the tests were performed was selected so as to be above or equal to the yield strain and below the fracture strain of the materials. Total separation or fracture of the specimen into two parts was considered as failure and the final life of the specimen. Stress-strain data was obtained to construct the hysteresis loops for analysis. The plastic strain computed from the hysteresis loop was given in Fig. 3 and calculated according to:

$$\Delta\varepsilon_{\mathrm{p}} = \Delta\varepsilon_{\mathrm{t}} - \frac{\Delta\sigma}{E} \tag{1}$$

where $\Delta\varepsilon_{\mathrm{p}}$ and $\Delta\varepsilon_{\mathrm{t}}$ are the plastic and total strain range, respectively, and $\Delta\sigma$ is the applied stress range which is taken from the half-life of the specimen (because no steady-state stress amplitude or saturation level was observed).

Tensile properties of the materials were also determined using the same specimen geometry, machine and

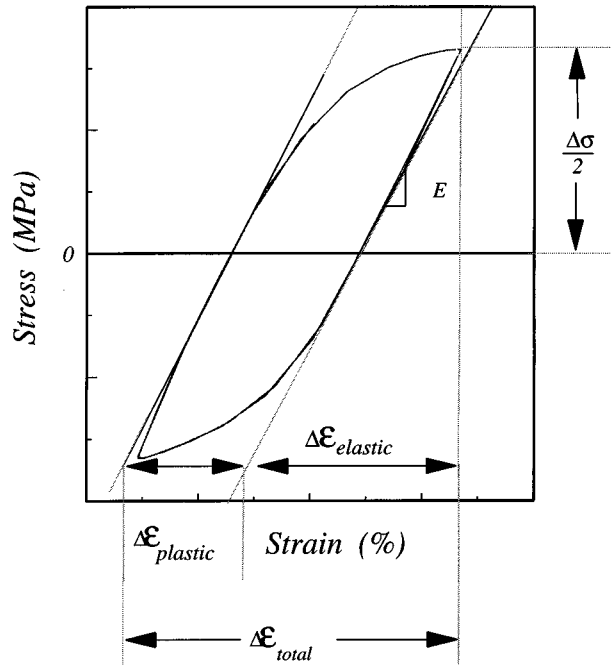


*Figure 3* The total strain, elastic strain and plastic strain from hysteresis loop.

extensometer as those for low cycle fatigue tests. The fracture surfaces of the LCF specimens were examined using an optical stereo microscope and a scanning electron microscope (SEM) to determine the predominant fracture modes and fracture surface features.

## 3. Results

The tensile properties of the MMC materials are listed in Table I, where $n$ and $k$ are strain hardening exponent and strength coefficient, respectively, of the stress-strain equation: $\sigma = k\varepsilon^n$. Note that $\sigma_y$ was obtained at 0.2% offset.

The cyclic stress response of specimens subjected to plastic straining for D20 and C85 composites are shown in Figs 4 and 5 respectively. Each curve refers to the response of a single specimen subjected to half the total strain range ($\Delta\varepsilon_{\mathrm{t}}/2$) given. With D20, hardening occurs during the initial stage of cyclic deformation, followed by softening for most of the fatigue life. In C85 a period of rapid initial softening during the first few cycles of straining was observed. This period was followed by progressive softening for most of the fatigue life and then immediately prior to failure a rapid drop in cyclic stress due to crack growth in the material. The cyclic response curves demonstrate generally, three stages in both materials, firstly fast hardening or softening in the first few cycles, secondly gradual softening for most of the fatigue life in which the stabilisation stage is not

TABLE I Tensile properties and LCF parameters of tested MMCs

| Material (T6 condition) | $E$ GPa | True UTS MPa | True $\sigma_y$ MPa | $\varepsilon_{\mathrm{f}}$ % | $n$ | $k$ MPa | $c$ | $n'$ | $k'$ MPa |
|---|---|---|---|---|---|---|---|---|---|
| D20 | 92.6 | 374 | 339 | 2.9 | 0.162 | 961 | −0.67 | 0.146 | 869 |
| C85 | 89 | 365 | 320 | 3.6 | 0.152 | 643.5 | −0.75 | 0.140 | 824 |

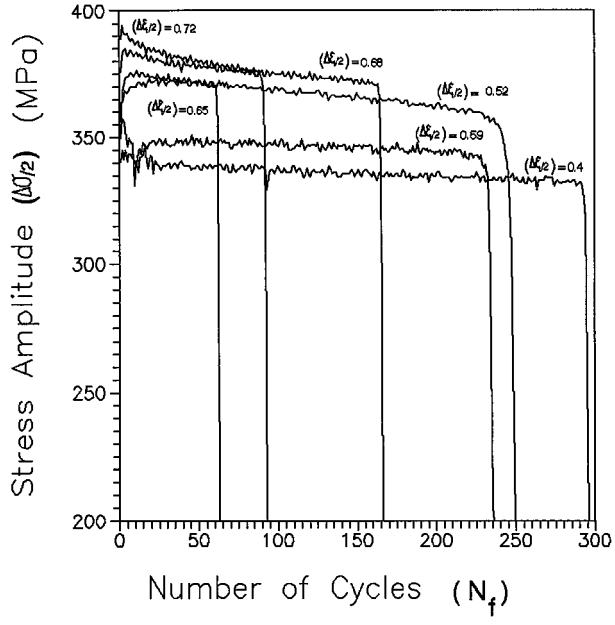


*Figure 4* Cyclic stress response ($\Delta\sigma/2$) of D20 specimens subjected to the total strain range ($\Delta\varepsilon_t/2$) indicated.

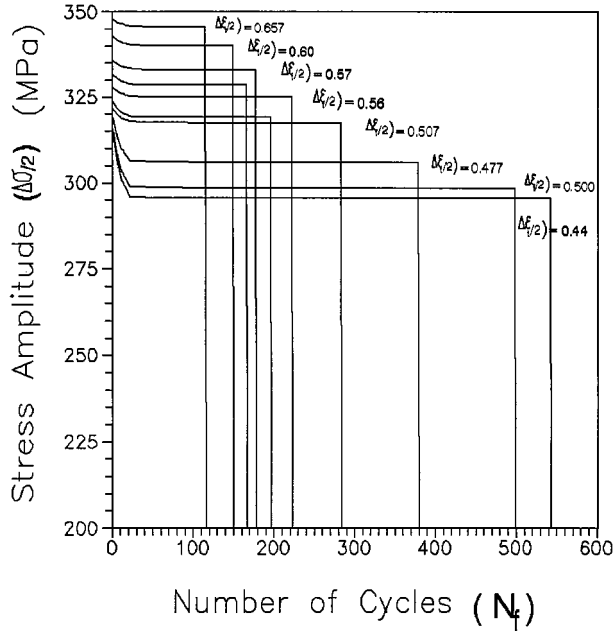


*Figure 5* Cyclic stress response ($\Delta\sigma/2$) of C85 specimens subjected to the total strain range ($\Delta\varepsilon_t/2$) indicated.

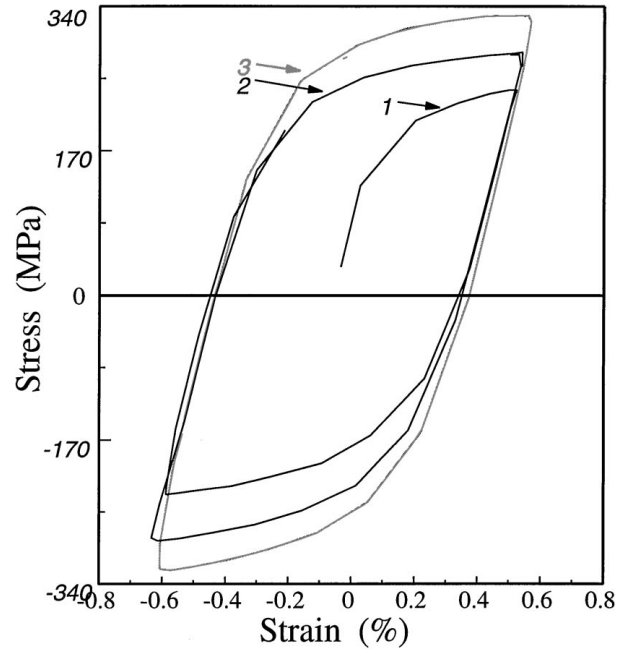


*Figure 6* Hysteresis loop of D20 specimen at the first, second and third straining cycle showing fatigue hardening.

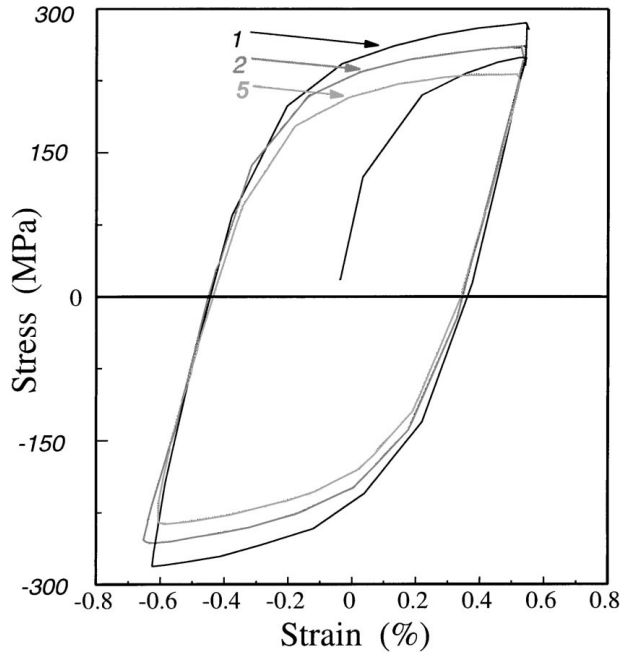


*Figure 7* Hysteresis loop of C85 specimen at the first, second and third straining cycle showing fatigue softening.

clear and finally a rapid drop in stress carrying capability prior to failure. As shown in Figs 4 and 5 the average peak stress versus number of cycles relationship depends strongly on the level of the total strain range applied.

The hysteresis loops for D20 and C85 composites are shown in Figs 6 and 7 respectively. When the hysteresis loops for these materials were closely examined, the above three different stages were recognised again. The hysteresis loops for both materials were symmetrical in the early stages where hardening or softening took place and also in the second stage.

The cyclic stress-strain curves could be obtained from a series of strain-controlled tests at different strain amplitudes. These curves describe the relation between cyclic flow stress and cyclic plastic strain amplitude, and can be expressed by a power function i.e.

$$\frac{\Delta\sigma}{2} = k'\left(\frac{\Delta\varepsilon_p}{2}\right)^{n'} \tag{2}$$

where $\Delta\sigma/2$ is the steady-state stress amplitude, $\Delta\varepsilon_p/2$ is the cyclic plastic strain amplitude, $n'$ is the cyclic strain hardening exponent which provides a measure of the material's response to cyclic strain and $k'$ is the cyclic strength coefficient. Since both materials show a changing stresses amplitude with increasing number of cycles, no steady-state stress amplitude (saturation level) could be achieved, $\Delta\sigma$ and $\Delta\epsilon_p$ are therefore both

taken at the fatigue half life of the specimens. Values of $k'$ and $n'$ are also given in Table I.

The number of cycles to failure as a function of plastic strain amplitude ($\Delta\varepsilon_p$) for D20 and C85 composites can be described by the Coffin-Manson relationship:

$$\frac{\Delta\varepsilon_p}{2} = \varepsilon_f'(2N_f)^c \tag{3}$$

where $\varepsilon_f'$ and $c$ are the fatigue ductility coefficient and fatigue ductility exponent respectively. Taking the logarithmic of both sides,

$$\log\left(\frac{\Delta\varepsilon_p}{2}\right) = \log\varepsilon_f' + c\log(2N_f). \tag{4}$$

Figs 8 and 9 plot the data according to Equation 4 which gives a linear relationship between $\log(\Delta\varepsilon_p)$ and $\log N_f$ for both composites. The slope of the straight line gives the fatigue ductility exponent $c$. Thus $c$ is $-0.67$ and $-0.75$ for D20 and C85 respectively. The corresponding values for $\varepsilon_f'$ are 0.12 and 0.09. Consequently at a given strain level the number of cycles required for failure of D20 was greater than C85 due to the slightly higher fatigue ductility coefficient $\varepsilon_f'$ and a lower fatigue ductility exponent $c$.

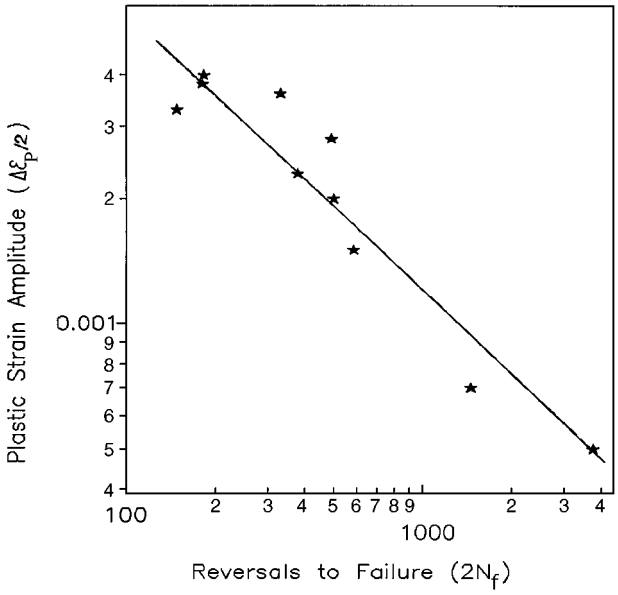


*Figure 8* Log-log plot number of cycles to failure ($N_f$) verses plastic strain amplitude ($\Delta\varepsilon_p/2$) for D20.

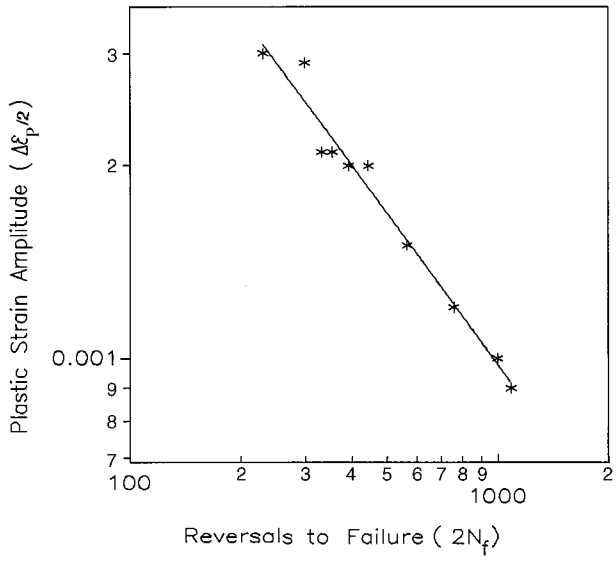


*Figure 9* Log-log plot number of cycles to failure ($N_f$) verses plastic strain amplitude ($\Delta\varepsilon_p/2$) for C85.

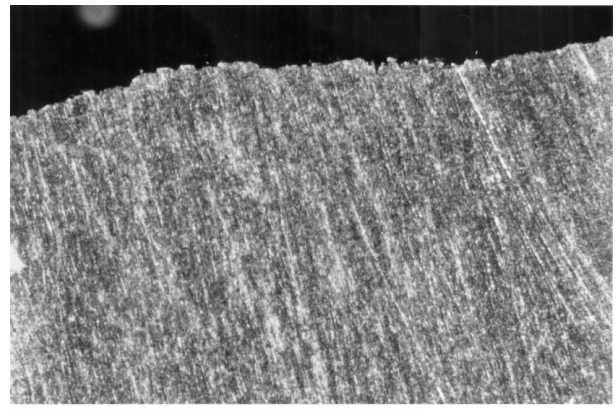

(a)

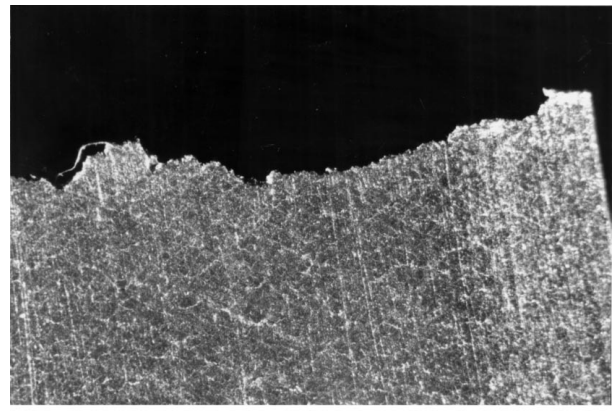

(b)

*Figure 10* a) Crack profile in a D20 specimen, fractured at high strain amplitude; and b) Crack profil in a D20 specimen, fractured at low strain amplitude.

Photographs were taken from crack profiles of LCF specimens fractured under cyclic plastic strains Figs 10 and 11. There is evidence of crack path dependence on strain amplitude. At high plastic strain amplitudes the crack profile is smooth with little shear in both MMCs (Figs 10a and 11a). At higher magnification, however, some micro-deflection of the crack was observed. Conversely, at low strain amplitudes, the crack path is rough and there is clear evidence of crack deflection during propagation (Figs 10b and 11b). In some areas the fracture path is at 45° to the applied stress, suggesting it fails by the maximum resolved shear stress. All specimens tested at low strain amplitudes for both materials show some degree of cracking at 45° to the crack plane.

Scanning electron micrographs of the fracture surfaces of the tensile and LCF specimens revealed ductile failure by nucleation and growth of voids. The fracture surfaces of all specimens showed dimples, i.e. a typical ductile fracture feature. Matrix dimpling was accompanied by particle fracture and debond from the metal/particle (m/p) interface. The initiation of fatigue cracks was always at a specimen edge where the surface

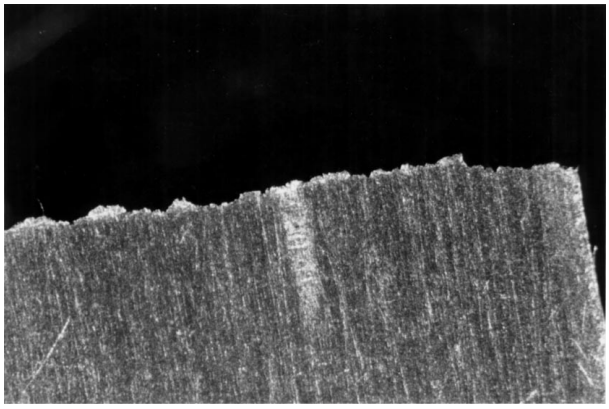

(a)

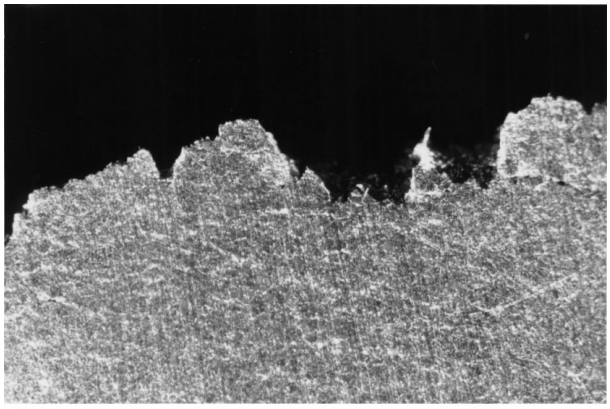

(b)

*Figure 11* a) Crack profile in a C85 specimen, fractured at high strain amplitude; and b) Crack profile in a C85 specimen, fractured at low strain amplitude.

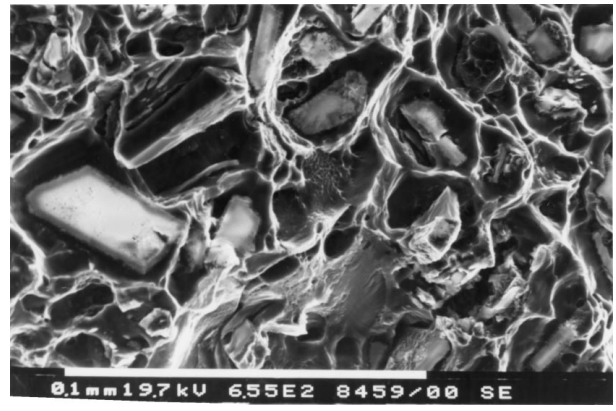


*Figure 12* Fracture surface of a D20 specimen, fractured at low levels of strain amplitude.

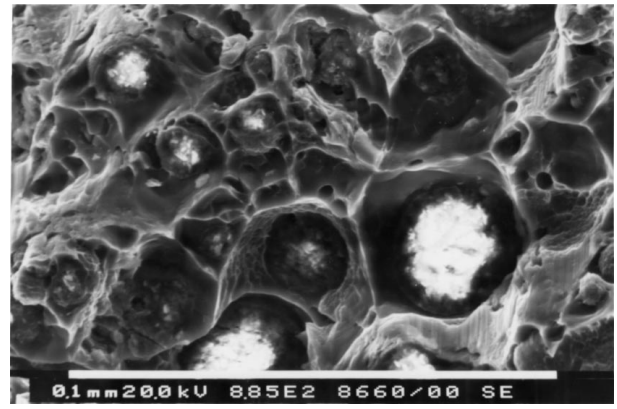


*Figure 13* Fracture surface of a C85 specimen, fractured at low levels of strain.

finish was at its worst. While initiation took place at several sites at high strain amplitudes, only one initiation site was found for specimens fractured at low strains. There are some differences between the fracture surface feature of specimens which fractured at high strains and those fractured at low strains in both MMC materials. The fracture morphology of specimens that fractured at low strains is essentially characterised by well formed voids centred around fractured and/or debonded particles with very thin matrix ligaments between the primary voids. Nucleation and growth of small secondary voids is observed in the matrix ligaments between the reinforcement. In contrast, fracture surfaces of specimens that fractured at high level of strain amplitudes, were covered with large and small shallow voids around the fractured and/or debonded particles. The matrix between neighbouring voids was ruptured by the formation of small dimples. Image analysis of fracture surfaces showed that while the area of the particles was 14.8% and 13.1% for D20 and C85 composites respectively at low strain amplitudes, it was 22.1% for D20 and 23.3% for C85 at high strain amplitudes.

Investigation of fracture surfaces of both materials showed that there were some differences in fracture morphology. While both displayed extensive shear deformation and drawing of matrix material to form shear lips between the alumina particles at low strain amplitudes, in D20 the matrix between alumina particles formed sharp shear lips with few small secondary dimples (Fig. 12), whereas in C85, primary dimples around alumina particles are separated by larger secondary dimples (Fig. 13). In addition, both fractured and debonded particles were observed in the two MMCs at high and low strain amplitudes. In the D20 material at low strains, most particles were damaged due to fracture and a small number of them debonded from the m/p interface. The observed number of m/p interface debonded particles was markedly higher in C85 at a similar level of straining. At high strain amplitudes, the number of debonded particles from m/p interface increased to approximately 10% in D20 and 7.2% in C85.

## 4. Discussion

Cyclic deformation plays an important role in crack nucleation and growth during the fatigue process. The cyclic strain response, which was measured during total strain-controlled fatigue, provides useful information in describing the behaviour of the material under cyclic strain. Irreversible deformation of the material is strongly influenced by variables such as alloy composition, microstructure and heat treatment condition, test condition and prior load history. Besides these factors, in MMC materials, other factors such as high dislocation density in the matrix due to thermal contraction mismatch between the reinforcement and matrix, m/p interface properties and accelerated aging are also

important in determining the LCF behaviour. The fatigue response of the two tested MMCs is discussed below with respect to some of these factors.

### 4.1. Fatigue response of MMCs (fatigue hardening/softening)

Monitoring the stress response of the specimens during total strain-controlled tests and also their hysteresis loops indicate that D20 and C85 show different responses to cyclic strain. While D20 showed cyclic hardening at the very first stage of deformation and then cyclic softening, C85 demonstrate cyclic softening from the first stage of loading. It has been observed [18,19] that the fatigue hardening and softening responses are strongly dependent upon material microstructure and heat treatment condition. Previous investigations [20] show that there are some differences in chemical composition of both reinforcement and matrix of D20 and C85. Therefore the different behaviour of these two composites could be related to their different chemical composition. Excessive amounts of secondary inclusions in C85 providing more misfit dislocations due to quenching, together with a different matrix composition, may lead to different atomic diffusion rates during ageing treatment compared to D20. Since the diffusion rate is a key factor in ageing reactions and accelerated ageing, different diffusion rates may cause slightly different ageing conditions which were reported [21] for these two materials leading to different LCF responses.

Experimental results indicate that the strain hardening/softening rate is maximum in the first few cycles. Although both composites did not exhibit complete saturation during cyclic deformation, their rate of cyclic softening progressively decreased with increasing number of strain cycles. Numerical analysis performed by Llorca *et al.* [16] shows the same behaviour for MMCs under cyclic deformation.

The basic mechanism leading to saturation hardening/softening is the changing of dislocation structure and dislocation movement barriers from one equilibrium position to another [18]. During fatigue hardening or softening the dislocation structure changes gradually from the initial position, which is dependent on microstructure of the material, to the saturation position. At saturation, the dislocation structure undergoes no further change, therefore the stress-strain response of the material is constant. No saturation phenomenon was observed in the tested MMCs. This can be attributed to the fact that any change in dislocation structure takes place gradually and over a large number of cycles. If crack growth starts in the specimen before the dislocation structure reaches the final equilibrium stage, the specimen will fail before showing saturation. The short LCF life of the tested MMCs provides further evidence of this phenomenon.

Fatigue softening typically occurs in hardened material by precipitation hardening. In these materials strength is controlled by the precipitate/dislocation interaction. Fatigue softening occurs by the gradual elimination of obstacles to the motion of the dislocations. A possible mechanism for the elimination of obstacles to dislocation movement is given as follows [18]. When dislocations pass through coherent or semi-coherent particles, the particles are split into segments, which are shifted along the slip plane. The repeated to-and-for motion of dislocations in cyclic deformation may thus reduce the average precipitate size to the point at which the precipitate becomes thermodynamically unstable and revert to solid solution.

Another possible explanation for fatigue softening comes from the pile-up of dislocations at the barriers during the first tensile part of the cycle thus decreasing the back stress for reverse flow [22]. In other words plastic relaxation occurs in MMCs during reversed loading as a consequence of the removal of Orowan loops, leading to fatigue softening.

The change in the dislocation substructure in the gauge length of a low cycle fatigue specimen during the initial fast softening stage could be the reason for fast softening. Increases in dislocation density and rearranged substructure into well developed veins and walls at the end of softening process have been observed [23] in LCF of steel specimens. During this stage, it is suggested that hardening processes due to increase dislocation density are suppressed by the dislocation multiplication operation which spreads to new areas during the first cycle. The change in softening rates after the first stage is related to formation of the soft low dislocation density channels and persistent slip bands (PSBs) within the matrix of hard veins [24]. Additionally, fracture or debonding of reinforcing particles could induce softening by reducing the amount of load carried by the material, and produce sites for the nucleation of voids within the matrix. This process is especially important to the final life just before failure.

### 4.2. Effect of strain amplitude

The results obtained in this work show a strong dependency of fatigue life and fatigue behaviour of tested MMCs on strain amplitude. Although both MMCs exhibit a change in stress amplitude with number of cycles it is less pronounced at low strains. In addition, depending on the level of the applied strain amplitude, the fatigue life and failure behaviour of these materials are varied. The higher the strain amplitude, the higher is the rate of decay and the lower the fatigue life. At low strain amplitude the crack profile shows some degree of deflection and 45° shear failure, but at high strain amplitude the crack path exhibits a smooth planer profile. As fatigue cracks pass through low particle density areas there is less m/p interface debonding at low strain levels. However as they pass through high particle density areas, more debonding at m/p interface and less plastic deformation in the matrix metal at high strain levels occur.

At high strain amplitudes a crack with a given size will have a larger fracture process zone than at low strain amplitudes. This large fracture process zone at high strain levels covers more reinforcing and secondary particles. Because the strain is higher at this stage, particles can be damaged easily and accelerate crack growth rate; whereas at low strains, these particles act as barriers to crack growth. Hence, the weaker barriers which

could arrest crack growth at a low strain level cannot have the same effect as at a high strain level.

Since at high strain amplitude cracks start from more than one site, crack growth occurs by coalescing with other cracks. Therefore crack growth is fast. At low strains, the weakened barriers such as reinforcing particles can arrest the growing crack and deflect it. Crack deflection due to reinforcement particles produces rough fracture surfaces and crack profiles leading to increased crack closure. The roughness of the cracked surface represents a greater degree of closure and this can reduce crack growth rates especially at lower strain amplitudes when the crack opening displacement is small compared to the surface roughness.

One possible reason for the different behaviour of the materials at different strain amplitudes might be the change in dislocation substructure with increasing plastic strain. Saxena and Antolovich [25] have reported this change in copper polycrystals. The change in dislocation substructure features at high and low strain amplitudes was observed by Davidson *et al.* [26] in low carbon steel and by Roven [23] in mild steel. However, we have not yet done any work on the two tested MMCs to confirm this explanation.

### 4.3. Effect of matrix composition and reinforcement shape

It is apparent that D20 is slightly superior in low cycle fatigue than C85 with a somewhat longer fatigue life at a given strain amplitude. Also the micromechanisms of crack growth are different in these two MMCs. While at low strain amplitudes the fracture mechanisms are governed by fractured particles, m/p interface debonding also has an important role in the failure of C85. Although at high strain levels both materials show an increase in m/p interface debonding, this increase is greater in D20. It seems that the difference in the fatigue properties of D20 and C85 composites is due to the difference in microstructure of these materials.

Chemical analyses of both D20 and C85 [20] show additional amounts of iron, silicon and chromium in the C85 material compared to D20. For C85 the presence of Fe impurities leads to the formation of weak inclusions that change the material properties under monotonic and cyclic deformation. Iron-rich inclusions, which are potential void nucleation sites, damage at low strain amplitudes and cause the material to fail early. Fracture mechanism analysis [20, 27] and fractography results show large and deep voids around damaged alumina particles which grow with further straining. With increasing local strain second phase particles start to produce secondary voids within the ligament between the primary voids. This reduces available space for primary void growth and prevents further deformation. The existence of Si in the reinforcement particles in C85 together with additional iron in the matrix produce weaker m/p interfaces in this material compared to D20. Therefore the observed lower cyclic life in the C85 composite is ascribed to the synergistic influence of coarse iron-rich second phase particles and weak m/p interface.

The difference in particle morphology is another factor affecting the behaviour of these materials. The angular particles in D20 have higher stress concentration compared to the spherical reinforcement in C85. This gives a higher stress level near particles in D20 leading to more particle fractures than in C85.

### 4.4. Fatigue damage and crack initiation

Investigation of fracture surface and crack profile of the failed LCF specimens indicates that the crack almost always started from the specimen edge, where the surface finish was worst. These observations show that the effective local strain raisers in the edge surface region was somewhat higher than the reinforcement particles and secondary particles in the interior. Levin *et al.* [13] showed by finite element simulation that the reinforcement particles intersected by free surfaces are subjected to a higher stress than particles which are completely embedded in the matrix. The magnitude of this increase exceeds 1.5 times. Also, the magnitude of strain in the matrix near the particles is higher at the free surface than in the interior of material. The maximum local strain in the matrix region of the MMC material reaches a level much higher than that which would occur in an unreinforced matrix strained to an equivalent strain level [28], due to stress concentration by particles or the development of a large triaxial stress in the ductile matrix of composite as a result of constrained matrix plastic flow between reinforcement particles [29]. Therefore the crack resistance of the material decreases, and crack growth is enhanced and takes place from particle to particle by fracturing or debonding along the soft matrix until the final stage when the crack grows by rapid failure.

## 5. Comparison with other LCF data

Fig. 14 shows a comparison between results of this work and other results for 6061 aluminium based particulate

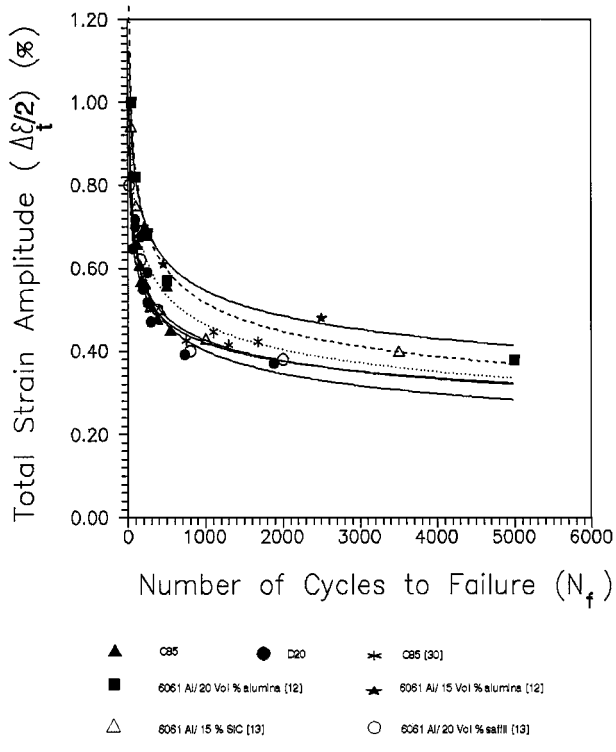


*Figure 14* Comparison results obtained in this work with other published data.

MMCs in peak-aged condition obtained from the literature. There is good agreement between all results cited and this work. All the experiment data show the same trend and exhibit an inverse power law relationship between total strain amplitude and number of cycles to failure. At high strain levels when the number of cycles to failure is less than 500 there is little difference between the data. At low strain levels when the number of cycles to failure is grater than 1000, 6061 Al/15 vol% alumina [12] has better fatigue life a at given total strain. C85, D20 and 6061 Al/20 vol% Saffil fibres [13] show very similar behaviour. The results for 6061 Al/15 vol% SiC [13] and 6061 Al/20 Vol% alumina [12] lie slightly below the result of 6061 Al/15 vol% alumina and slightly above results of D20 and C85. It seems that the low cycle fatigue behaviour of these MMCs is largely dependent on the ductility of the material. Therefore D20, C85 and 6061 Al/20 vol% saffil with elongation to failure of 3.6%, 3.2% and 3.1% respectively, have similar but lower resistance to low cycle fatigue when compared to 6061 Al/15 vol% alumina [12] with an elongation to failure of 5.1%.

## 6. Conclusions

(a) Under cyclic plastic straining both D20 and C85 composite in peak-aged condition display a short cycle fatigue life. However, D20 has a slightly superior low cycle fatigue resistance to C85.

(b) The LCF life of both composites may be assessed according to the Coffin-Manson type relationship.

(c) Results indicate that D20 and C85 composites exhibit different responses to cyclic plastic straining. D20 demonstrates cyclic hardening during the initial stage of cyclic deformation, followed by softening and near-cyclic stability; whereas C85 shows a period of rapid initial cyclic softening during the first few cycles and then slow softening for most of the fatigue life.

(d) Both MMCs shows three stages in their response to LCF: firstly, fast hardening (D20) or softening (C85) in the first few cycles; secondly, gradual softening for most of the fatigue life; and finally, a rapid drop in the stress carrying capability prior to failure.

(e) Although all fracture specimens loaded by cyclic strain show typical ductile fracture features consisting of nucleation and growth of voids, it was observed that the applied strain amplitude has a strong influence on the crack path, surface fracture morphology and fracture behaviour of the tested MMCs.

## Acknowledgements

The authors would like to thank the Australian Research Council and Shiraz University, Shiraz, Iran for the financial support of this project.

## References

1. M. J. HADIANFARD, G. HENESS, J. C. HEALY and Y.-W. MAI, *Fatigue Fract. Engng. Mater. Struct.* **17** (1994) 235.
2. N. E. FROST, K. J. MARSH and L. P. POOK, "Metal Fatigue" (OUP, 1974) p. 42.
3. J. LANKFORD, *Int. Metals Review* **220** (1977) 221.
4. D. BROOKSBANK and K. W. ANDREWS, *JISI* **210** (1972) 246.
5. J. F. KNOTT and J. E. KING, *Materials & Design* **12** (1991) 67.
6. H. TODA and T. KOBAYASHI, *Metall. Mate. Trans.* **A27** (1996) 2013.
7. N. J. HURD, *Mater. Sci. Tech.* **4** (1988) 513.
8. D. F. HASSEN, C. R. CROWE, J. S. AHEARN and D. C. COOKE, in "Failure Mechanisms in High Performance Materials," edited by J. G. Early, T. R. Shives and J. H. Smith (1984) p. 147.
9. B. HARRIS, *Mater. Sci. Tech.* **4** (1988) 231.
10. N. OTANI and D. SONG, *J. Mate. Sci.* **32** (1997) 755.
11. S. Q. GUO, Y. KAGAWA and K. HONDA, *Metall. Mate. Trans.* **A27** (1996) 2843.
12. C. C. PERNG, J. R. HWANG and J. L. DOONG, *Comp. Sci. and Tech.* **49** (1993) 225.
13. M. LEVIN and B. KARLSSON, *Int. J. Fatigue* **15** (1993) 377.
14. R. T. BHATT and H. H. GRIMES, *ASTM-STP* **732** (1981) 274.
15. J. ROBLES, K. R. ANDERSON, J. R. GROZA and J. C. GIBELING, *Metall. Trans.* **A25** (1994) 2235.
16. J. LLORCA, S. SURESH and A. NEEDLEMAN, *Metall. Trans.* **A23** (1992) 919.
17. D. M. ELZEY and E. ARZT, *Metall. Trans.* **A22** (1991) 837.
18. M. KLESNIL and P. LUKAS, in "Fatigue of Metallic Materials" (Elsevier Scientific Publishing Company, Amsterdam, 1980) p. 12.
19. T. S. SRIVATSAN, D. LANNING and K. K. SONI, *Int. J. Fatigue* **15** (1993) 231–242.
20. M. J. HADIANFARD, J. C. HEALY and Y.-W. MAI, *J. Mat. Sci.* **28** (1993) 6217.
21. M. J. HADIANFARD, PhD thesis, Sydney University, Australia, 1995.
22. M. JAIN, *Fract. Engng. Mater. Struct.* **33** (1992) 42.
23. H. J. ROVEN and E. NES, *Acta, Metall. Mater.* **39** (1991) 1719.
24. H. MUGHRABI, *Mater. Sci. Engng.* **33** (1978) 207.
25. A. SAXENA and S. D. ANTOLOVICH, *Metall. Trans.* **A6** (1975) 1809.
26. D. L. DAVIDSON, J. LANKFORD, T. YOKOBORI and K. SATO, *Int. J. Fract.* **12** (1976) 579.
27. M. J. HADIANFARD, J. HEALY and Y.-W. MAI, *J. Mat. Sci.* **29** (1994) 2321.
28. P. MCHUGH, R. J. ASARO, C. F. SHIH, and A. G. VARIAS, in Proceedings 10th Int. Symp. on Metallurgy and Materials Science, RISO National Laboratory, Roskilde, Denmark, 1989, p. 129.
29. T. CHRISTMAN and S. SURESH, *Mater. Sci. Engng.* **A102** (1988) 211.
30. R. E. ALLSOPP, BE Thesis, University of Sydney, 1992.

*Received 31 July 1998*
*and accepted 30 September 1999*